Electronic Supplementary Material (ESI) for Physical Chemistry Chemical Physics.

The influence of strontium deficiency on thermodynamics of defect formation, structural stability and electrical transport of $SrFe_{0.5}Ta_{0.5}O_{3-\delta}$ based solid solutions with an excess tantalum content

B.V. Politov[1,2]*, J.C. Waerenborgh[3], I.R. Shein[1], O.V. Merkulov[1]

[1] *Institute of Solid State Chemistry, UB RAS, 620990 Ekaterinburg, Russia*

[2] *Institute of Solid State Chemistry and Mechanochemistry, SB RAS, 630128 Novosibirsk, Russia*

[3] *C2TN, Instituto Superior Técnico, Universidade de Lisboa, E.N. 10 ao km 139,7, 2695-066 Bobadela LRS, Portugal*

* Corresponding author. Tel: +7-343-3623164; Fax: +7-343-3744495;

E-mail: politoffboris@yandex.com

SUPPLEMENTARY INFORMATION FILE

Methodology of defect formation calculations

The determination of actual values of defect formation enthalpy in disordered materials in the course of DFT + U simulations is in general a time-consuming problem. In order to overcome these limitations the following procedure was applied for each defect type in this work. Firstly, the crystal geometry of cation-ordered tetragonal SFT50 oxide was precisely calculated. Secondly, the obtained unit cell was converted using VESTA software into either 120- or 360-atomic supercell where all tantalum atoms were replaced with iron atoms. After that, a special procedure (as implemented in vaspkit program package [S1]) was applied so that to generate SFT50 alloy containing tantalum and iron atoms in a ratio 50:50 in close to random arrangement. For each supercell size three individual configurations were created, which were thoroughly relaxed and their total energies were subsequently calculated; the ones with the lowest energy were chosen for further manipulations. Thirdly, the detailed list of oxygen positions (covering both crystallographic and atomic environment) was made for each supercell based on the atomic geometry obtained during the respective relaxation procedure. Similar lists were made for cation species. Accordingly, single defects were modeled by a random removal of oxygen atoms in specific coordination or metal atoms in their regular positions; the procedure described was realized by a specially written script that was able to randomly pick a desired atom from a corresponding list belonging to a supercell of interest. For each defect type three new supercells were produced; these were properly relaxed and their total energies were determined. The respective enthalpy of formation was estimated for the supercell with the lowest total energy.

Finally, the simultaneous presence of two defects was modeled only for 360-atomic supercell. The initial configuration for these calculations was chosen based on the results of previous step. Further on, the new defect was added in accord with the procedures described above, again producing three new supercells. Each of them was relaxed and the one with the lowest energy was used for the evaluation of defect formation enthalpy. The scheme presented here is schematically shown in figure S1 for one of the tested supercells.

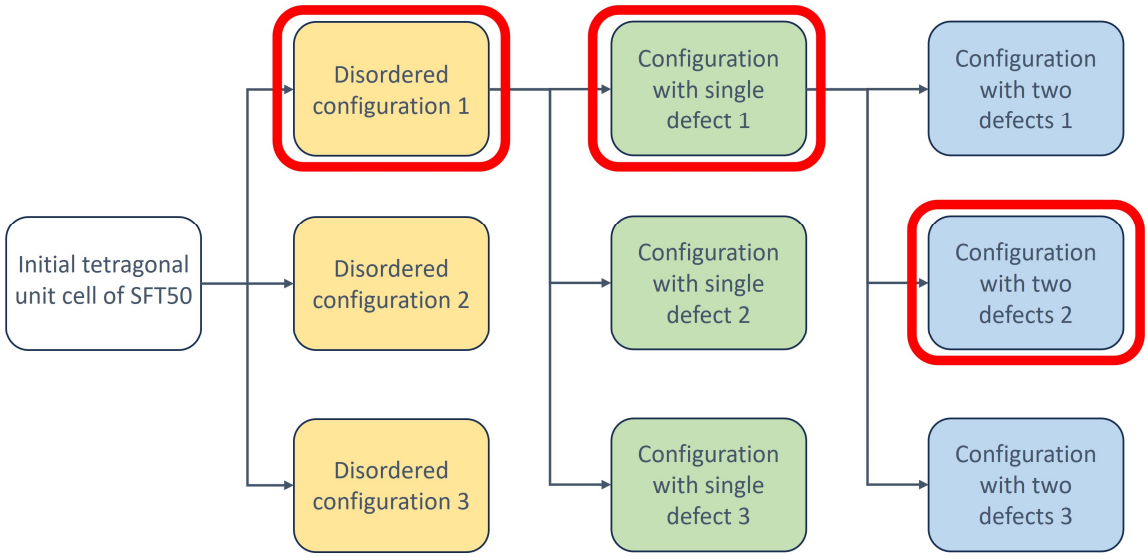

Fig. S1. Flowchart of calculation procedure for determining the enthalpy of defect formation in SFT50-based materials. Red frames designate the calculated configuration with the lowest total energy among considered.

Table S1. The results of EDX analysis for $SrFe_{0.5-x}Ta_{0.5+x}O_{3-\delta}$ and $Sr_{1-x}Fe_{0.5-x}Ta_{0.5+x}O_{3-\delta}$ series of ceramic samples. The values in brackets represent the nominal metal content in a specimen.

Element	Element concentration in sample, at. %				
	SFT50	SFT55	SFT60	SFT55’	SFT60’
Sr	49.6 ± 1.2 (50)	48.9 ± 1.3 (50)	47.8 ± 1.3 (50)	49.1 ± 1 (48.7)	46.9 ± 1.4 (47.4)
Fe	28.7 ± 1.4 (25)	27.8 ± 2 (22.5)	25.1 ± 0.8 (20)	26.4 ± 1.2 (23.1)	25.6 ± 0.6 (21)
Ta	21.6 ± 0.9 (25)	22.6 ± 2 (27.5)	27.1 ± 0.9 (30)	24.4 ± 0.7 (28.2)	27.5 ± 0.5 (31.6)

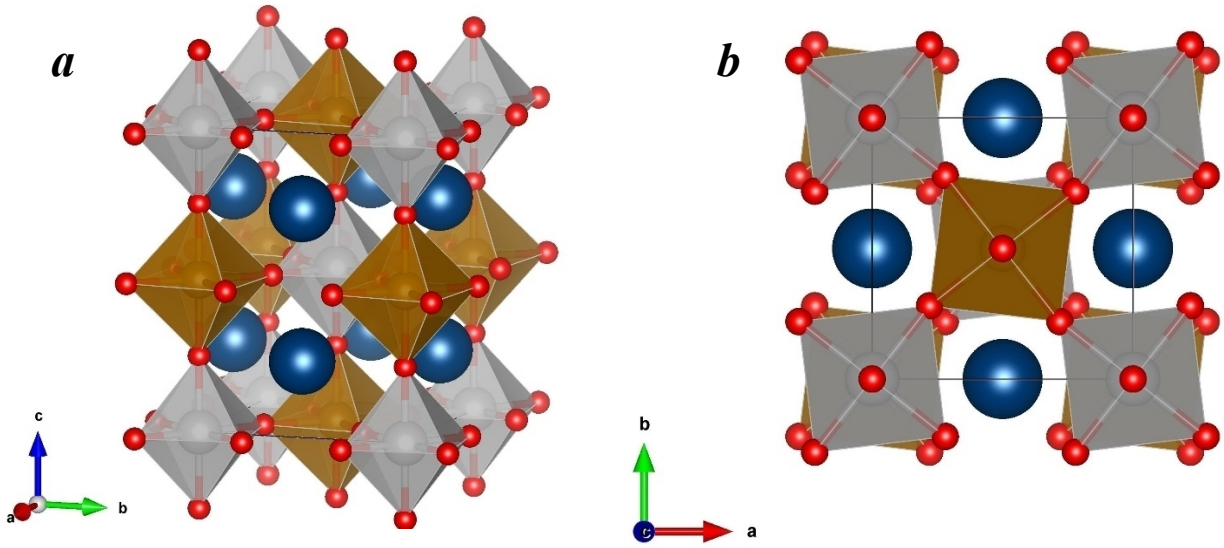

Fig. S2. Schematical depiction of $SrFe_{0.5}Ta_{0.5}O_3$ structure used in DFT + U calculations shown in two different projections. Strontium atoms are depicted with dark blue spheres, oxygen atoms – with red spheres. Grey polyhedra represent TaO_6 octahedra, brown – FeO_6 octahedra.

Table S2. The mechanical constants calculated via the DFT + U method for cation-ordered orthorhombic SFT50 oxide. The mechanical stability criteria for orthorhombic crystals are taken from work [S2].

Elastic constant	Value, GPa	Stability criterion	Value, GPa	Condition fulfilled?
C_{11}	3.125	$C_{11} > 0$	3.125	yes
C_{22}	3.359	$C_{22} > 0$	3.359	yes
C_{33}	3.208	$C_{33} > 0$	3.208	yes
C_{44}	1.180	$C_{44} > 0$	1.180	yes
C_{55}	1.120	$C_{55} > 0$	1.120	yes
C_{66}	1.255	$C_{66} > 0$	1.255	yes
C_{12}	0.825	$C_{11} + C_{22} - 2C_{12} > 0$	4.835	yes
C_{13}	0.933	$C_{11} + C_{33} - 2C_{13} > 0$	4.467	yes
C_{23}	0.818	$C_{22} + C_{33} - 2C_{23} > 0$	4.931	yes
		$C_{11} + C_{22} + C_{33} + 2(C_{12} + C_{13} + C_{23}) > 0$	14.845	yes

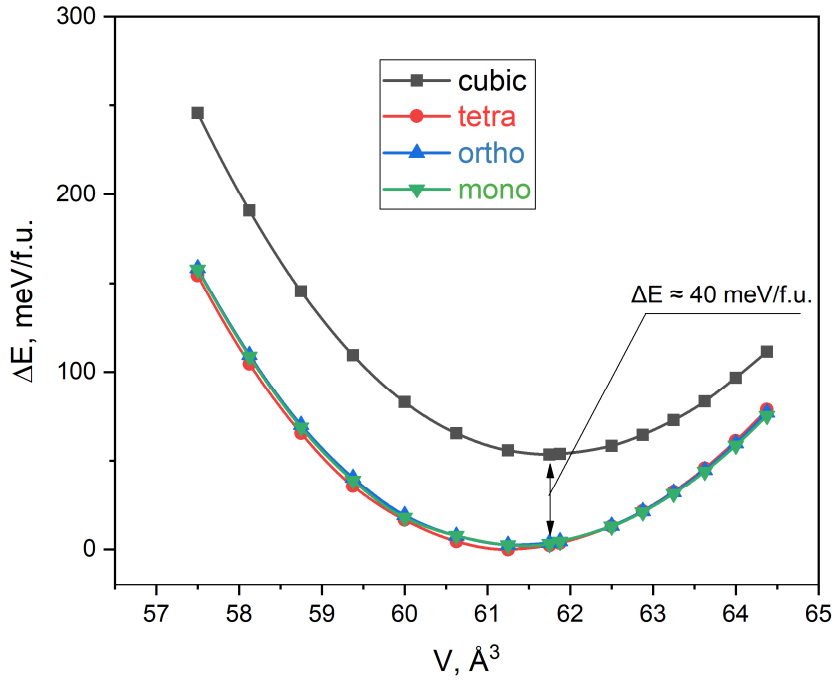

Fig. S3. Relative changes ΔE of total energies of SFT50 unit cells (represented in meV/f.u.) with different crystal symmetries as obtained in the course of SCAN calculations at variable volume V. The corresponding ΔE difference between cubic and other symmetries is also shown.

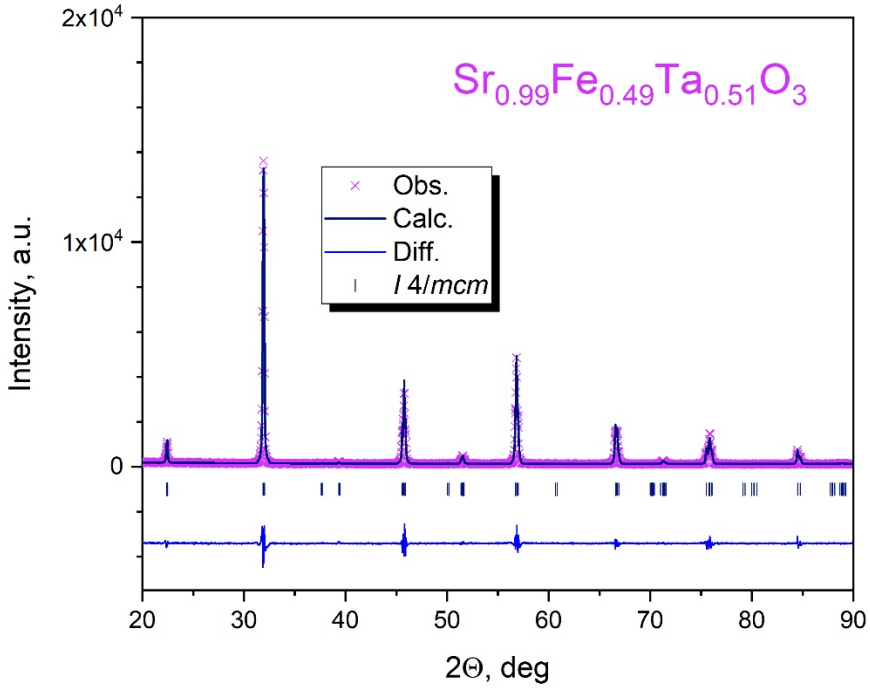

Fig. S4. The experimental (crossed symbols) and calculated using the Rietveld refinement procedure (dark blue lines) XRD patterns of SFT51' oxide. The difference between theory and experiment along with the reflection positions are also supplied within the figure.

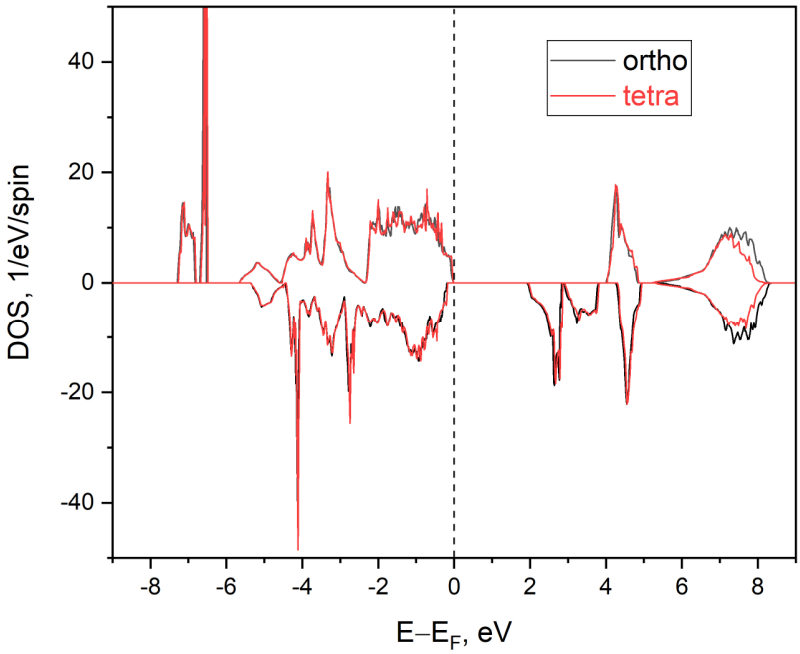

Fig. S5. The DOS spectra calculated with the help of DFT + U formalism for SFT50 with tetragonal and orthorhombic lattice symmetries. Negative values show the spin-down states, Fermi level is marked with a vertical dashed line.

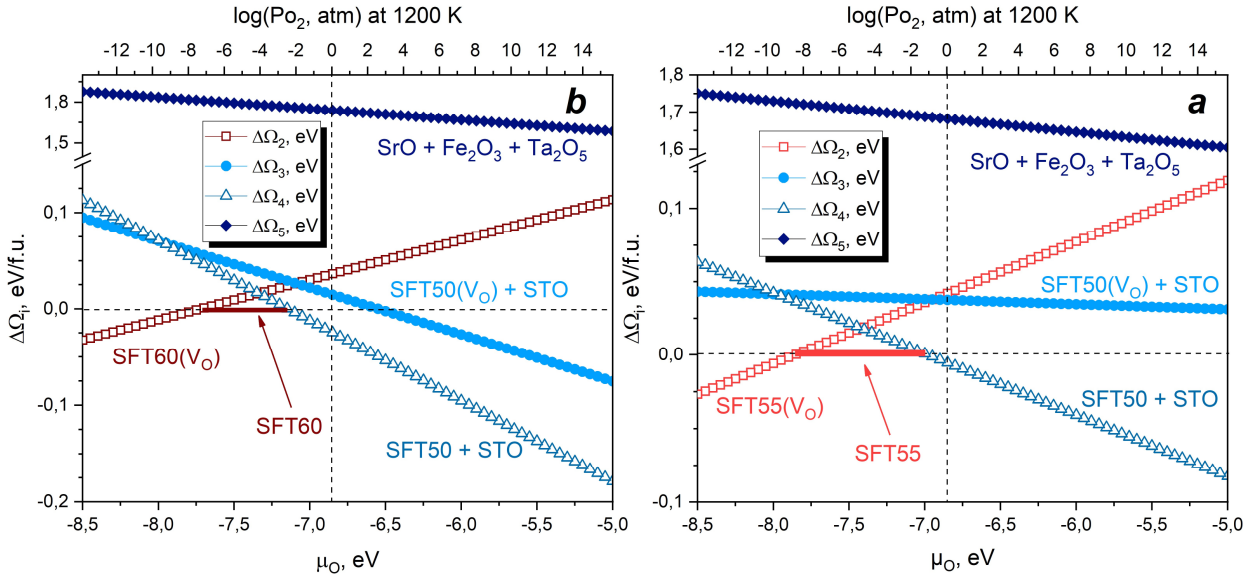

Fig. S6. Thermodynamic stability of oxide compositions with cation stoichiometries corresponding to SFT55 (*a*) and SFT60 (*b*) oxides, calculated using grand thermodynamic potential method. The particular Ω_i values are shown relative to Ω_1 which is computed for a pure perovskite-like phases $SrFe_{0.5-x}Ta_{0.5+x}O_3$ which is marked by a dashed horizontal line. The upper abscissa axis shows the values of oxygen partial pressure at 1200 K that are equivalent to oxygen chemical potential μ_O at similar conditions; 1 atm pressure is given by a vertical dashed line. The effects of non-ideality of oxygen gas at high pressures are omitted.

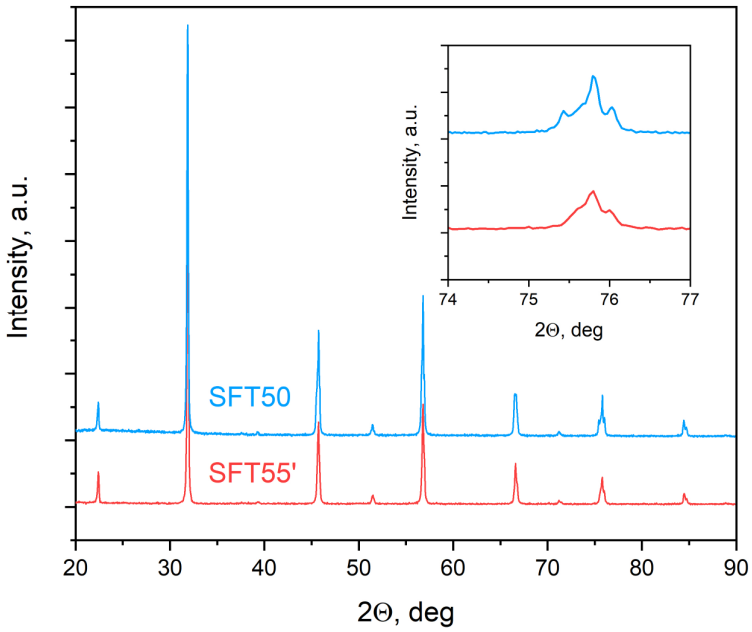

Fig. S7. The experimentally obtained XRD patterns for SFT50 and SFT55' oxides quenched from air at 1373 K to liquid nitrogen. The inset shows enlarged data at high angles.

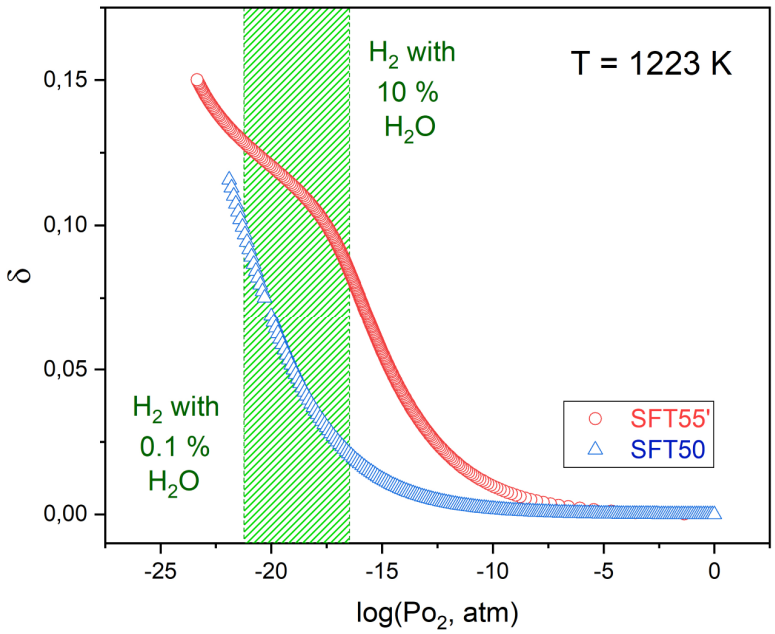

Fig. S8. Oxygen non-stoichiometry in SFT50 and SFT55' oxides calculated at 1223 K as a function of oxygen partial pressure. The dashed rectangle shows the interval of possible Po_2 values in a humidified hydrogen.

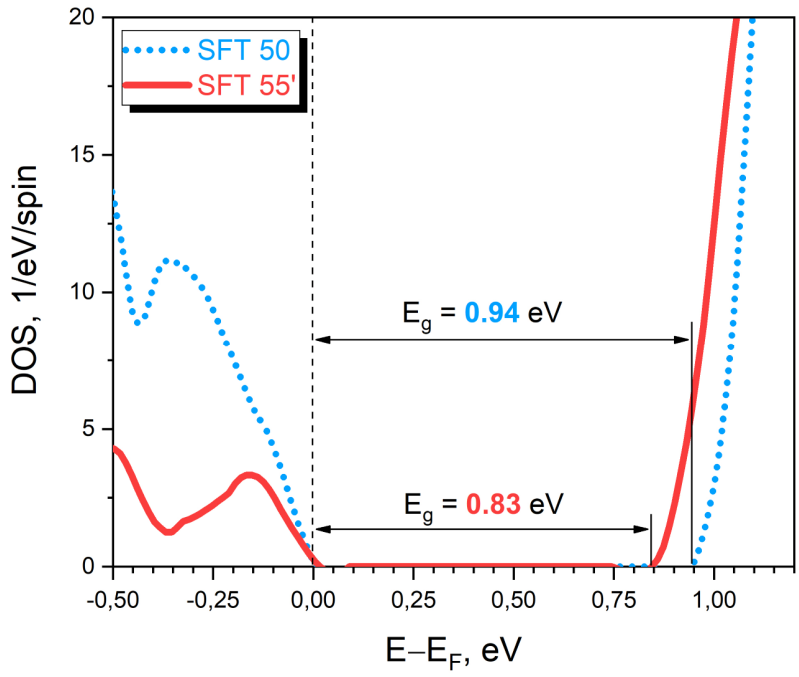

Fig. S9. Band structure of SFT50 and SFT55' oxides in the vicinity of Fermi level E_F calculated using DFT + U approach. The actual position of E_F is shown with a vertical dashed line. The obtained band gap values are also supplied within the figure.

References

S1. Wang, V.; Xu, N.; Liu, J. C.; Tang, G.; Geng, W. T.; VASPKIT: A user-friendly interface facilitating high-throughput computing and analysis using VASP code. *Computer Physics Communications* **2021**, 267, 108033.

S2. Wu, Z. J.; Zhao, E. J.; Xiang, H. P.; Hao, X. F.; Liu, X. J.; Meng, J.; Crystal structures and elastic properties of superhard IrN_2 and IrN_3 from first principles. *Physical Review B* **2007**, 76 (5), 054115.